Applied Physics A (2022) 128:595
https://doi.org/10.1007/s00339-022-05704-9

Applied Physics A
Materials Science & Processing

Optimization strategy for green synthesis of silver nanoparticles (AgNPs) as catalyst for the reduction of 2,4-dinitrophenol via supported mechanism

Ahmed M. Abu-Dief[1,2] · Laila H. Abdel-Rahman[2] · M. A. Abd–El Sayed[3] · Mallak Megalea Zikry[3] · Mohamed E. Khalifa[5] · Nashwa M. El-Metwaly[4,6]

Received: 17 December 2021 / Accepted: 17 May 2022 / Published online: 20 June 2022

Abstract

Here, we examine the biogenic fabrication of silver nanoparticles (AgNPs) utilizing a simple and environmental friendly method. Silver nanoparticles were synthesized using medicinal plants extracts such as Flamboyant (*Delonix regia (*DRE)) and *Moringa oleifera* (MOE). The maximum absorbance (λ_{max}) of UV–Vis. analysis at 442 and 459 nm indicates the formation of MOEAgNPs and DREAgNPs, respectively. The AgNPs are confirmed by UV–Vis spectroscopy, Fourier transform infrared spectroscopy (FT-IR), Transmission Electron Microscopy (TEM) and XRD techniques. (FT-IR) FT-IR spectra indicate the functional groups of phytochemical compounds in silver nanoparticles (DREAgNPs, MOEAgNPs). The generation of spherical MOEAgNPs and DREAgNPs with a majority particle size of 50 and 100 nm, respectively, was confirmed by TEM analysis. The XRD pattern of AgNPs has FCC form and crystalline lattice at 2θ of 38°, 44°, 64° and 77° corresponding to (111), (200), (220), and (311) reflections of AgNPs. The findings indicate that the ideal conditions for the synthesis process were 2 mMAg^+ concentration, reaction time is 24 h and 60 °C for extraction. The reduction of 2,4-dinitrophenol to 2,4-diaminophenol using $NaBH_4$ was carried out under the catalytic influence of AgNPs. The rate constant k (1st cycle) was found to be 42×10^{-3} min^{-1} and 26×10^{-3} min^{-1} for the reaction in presence of MOEAgNPs and DREAgNPs, respectively. The recyclability of the prepared AgNPs was tested for 7 cycles without loss in its activity until cycle 5. The activation energy (E_a) for reduction of 2,4-dinitrophenol that catalyzed by MOEAgNPs or DREAgNPs, respectively, was 36.4 or 31.7 $kJmol^{-1}$. The successes of AgNPs in the catalytic role were supported through DFT studies.

✉ Ahmed M. Abu-Dief
ahmed_benzoic@yahoo.com;
amamohammed@taibahu.edu.sa

✉ Nashwa M. El-Metwaly
n_elmetwaly00@yahoo.com

[1] Department of Chemistry, College of Science, Taibah University, Madinah 344, Saudi Arabia

[2] Department of Chemistry, Faculty of Science, Sohag University, Sohag 82534, Egypt

[3] Department of Medicinal and Aromatic Plants Researches, Horti. Res. Institute (H.R.I.), Agri. Res. Center (A.R.C.), Giza, Egypt

[4] Department of Chemistry, Faculty of Applied Science, Umm Al-Qura University, Makkah, Saudi Arabia

[5] Department of Chemistry, College of Science, Taif University, P.O. Box 11099, Taif 21944, Saudi Arabia

[6] Department of Chemistry, Faculty of Science, Mansoura University, Mansoura, Egypt

Graphical abstract

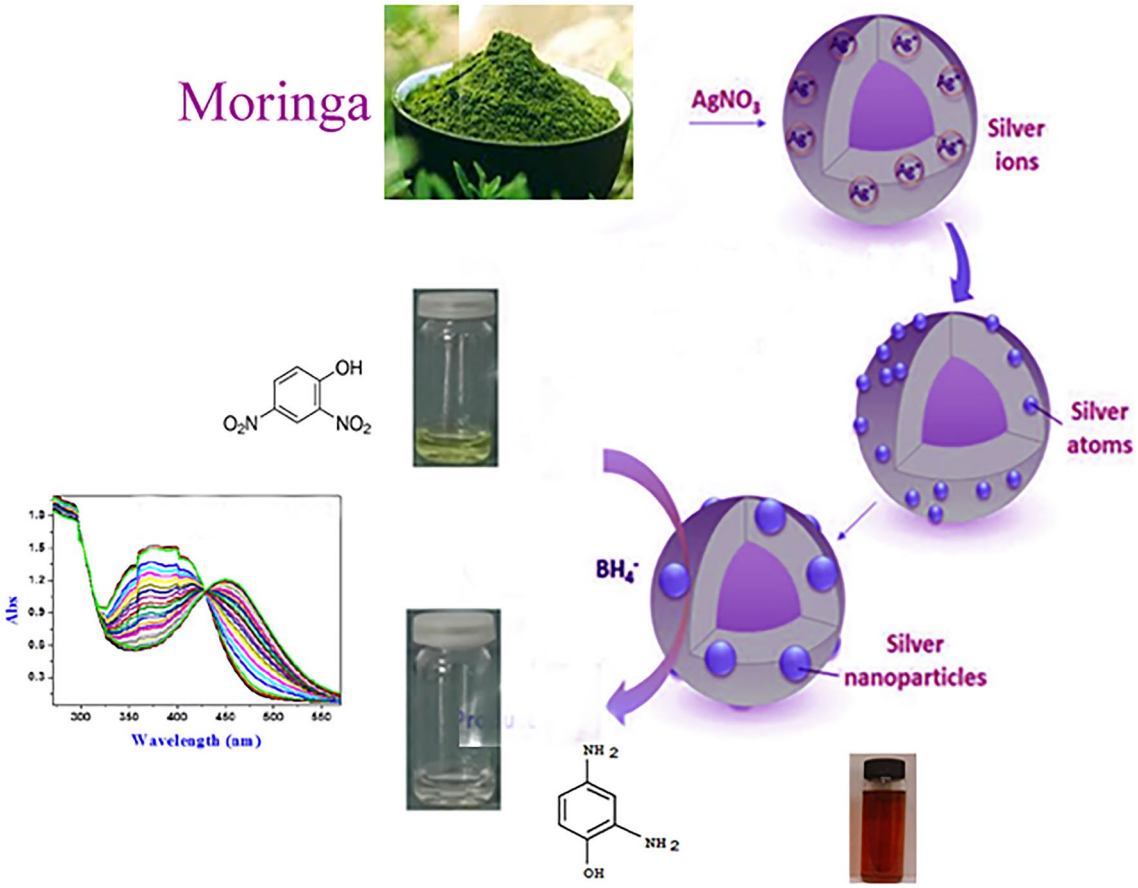

Keywords Silver nanoparticles · Catalytic reduction · 2,4-dinitrophenol · DFT-based mechanism

1 Introduction

Silver nanoparticles (AgNPs) are an essential material because of their advantages, such as low production costs and easy synthesis. The AgNPs have been used in a variety of applications, including catalysis, optical and electrical properties, as well as their potential as catalysts and sensors of nanomaterials were studied [1–4]. Chemical methods making metal nanoparticles are costly and not eco-friendly [5]. These processes have a number of disadvantages, including the use of poisonous solvents, the production of hazardous byproducts and high energy consumption. As a result, ecologically friendly approaches for the production of metal nanoparticles utilizing plant extracts are required. Ag and Cu nanoparticles exhibit antibacterial properties [6–8]. Because of their antibacterial and antiviral capabilities, copper nanoparticles are used for water purification, food processing, and other applications [9, 10]. AgNPs are commonly used in surgical device coatings, dental composites and bone prostheses due to their strong antibacterial and antifungal properties [11–13]. Also, used in food containers and air/water filters [14–16]. Furthermore, AgNPs are well-known redox catalysts that stimulate electron transfer via a distinct mechanism with low activation energy [17, 18]. The AgNPs synthesis is particularly essential because of its numerous industrial catalytic applications. One of the most extensively utilized green approaches for producing AgNPs is to use plant extracts as reducing agents and stabilizers [19–25]. Plants such as *Jatropha curcas* [26], *Capsicum annuum* [27], *Argemone mexicana* [28], *Ocimum sanctum* [29], *Ficus benghalensis* [30] and *Hibiscus rosa* Sinensis [31] have been effectively used to synthesize silver metal (Ag^0) nanoparticles from silver ions (Ag^+). It was investigated if decorating AgNPs onto photocatalysts may improve organics degradation during photocatalysis [32]. AgNPs were discovered to have a Fenton-like reaction, which allowed them to break down bisphenol in

water [33]. In previous researches, catalytic performance of gold nanoparticle and silver nanoparticle were evaluated in the reduction of 4-nitrophenol by $NaBH_4$. Xiao-Qiong Wu et al. have synthesized chitosan-Au hydrogel system via photoreduction and used it as reduction of nitrophenol derivatives by NaBH4. However, catalytic performance of neither sphere gold nor AgNPs have been evaluated through reduction of 2,4 -dinitrophenol (DNP), a derivative of aromatic nitro compounds, in the presence of $NaBH_4$. Only nickel particles decorated on electrospun polycaprolactone and chitosan-Au hydrogel system have been used for the reduction of DNP [34, 35]. In the presence of gold or silver nanoparticles, 2,4-dinitrophenol could be reduced to the equivalent 2,4-diaminophenol by $NaBH_4$ [36–43]. In this study, we aim to synthesize AgNPs by a green synthesis via using extracts from *M. oleifera* and *Delonix regia* [44, 45]. We choose *Moringa oleifera* and delonix regia as they are easily available in research stations in agricultural research center and the use of *Moringa oleifera* and delonix regia in the synthesis of silver nanoparticles is leading to truly green chemistry, which is more cost-effective and environmentally benign than chemical and physical methods because these plants are used as a traditional medicinal plant that provides better nourishment due to the presence of certain critical nutrients. Despite its potential as a future option for under nutrition therapy in clinical or biomedical settings, *Moringa oleifera* and delonix regia are required for the production of biomaterials or green materials in advanced bioengineering. The benefits of using these plants for the synthesis of nanoparticles are that the plants are possess a large variety of active functional groups that can promote the reduction of silver ions. Many researchers compared their extracellular synthesis of metallic silver nanoparticles using five plant leaf extracts (Pine, Persimmon, Ginkgo, Magnolia, and Platanus) [46]. From this point of view, our work will focus on green synthesis of AgNPs using economic and eco-friendly extracts of *Moringa oleifera* and delonix regia. The prepared AgNPs will be characterized via different techniques. After characterizing the nanoparticles produced, they will be used as a catalyst for reduction of 2,4-dinitrophenol by $NaBH_4$. The mechanism of catalysis was suggested according to DFT study on the expected intermediates.

2 Experimental methods

2.1 Material

Silver nitrate ($AgNO_3$), 2,4-dinitrophenol (2,4-DNP) and $NaBH_4$ were purchased from Sigma Aldrich with purity ≥ 99.8%, based on trace metal analysis.

2.1.1 Plant collection

M. oleifera and *Delonix regia* were collected from Sohag, Egypt (Shandaweel Research center). Plant extracts were used in the present study because it is proven to reduce silver ions.

2.1.2 Plant extract preparation

Fresh plants were picked and washed in bi-distilled water before being used. The leaves were broken into small pieces, and 30 g were weighed and put to 300 mL distilled water, which were then heated to 60 °C, filtered and stored at 4 °C. Notice: *M. oleifera* extract takes symbol MOE, while *Delonix regia* extract takes symbol DRE.

2.2 Preparation of Ag^+ *ions solution*

A stock solution silver ions was prepared from 0.85 g of $AgNO_3$ which dissolved to produce 5 mM concentration which, was then diluted to 1, 2 and 3 mM concentrations.

2.3 Synthesis of MOEAgNPs and DREAgNPs

Adding 20 mL of MOE to 180 mL from 2 mM $AgNO_3$ under constant stirring, the color changed from pale yellow to dark brown within 10 min, indicating the formation of MOEAgNPs and DREAgNPs which, were then collected by centrifuge.

2.4 Optimization conditions for AgNPs synthesis using aqueous extract of plant

The effect of various parameters on the synthesis of silver nanoparticles, such as the concentration of either silver nitrate concentration or plant extract, time of synthesis reaction and temperature, were evaluated using (DLS) measurements during the reaction time, as described in Table S1.

2.5 Characterization of AgNPs

The importance of characterization is to understand the shape and size of AgNPs. This characterization was carried out using UV–Vis spectroscopy, FT-IR and TEM. The descriptions of all techniques applied were elaborately typed in the supporting materials (part 1).

2.6 The catalytic reduction of 2,4-dinitrophenol

UV–Vis spectrophotometer was used to monitor this reduction reaction using 1.4 mL cuvette. [34]. A solution of 2,4-dinitrophenol (0.01 M) was prepared in ethanol. In presence of $NaBH_4$ with the absence of AgNPs catalyst, the

reduction of 2,4-dinitrophenol was tested. To assess AgNPs catalytic activity, the reduction process was conducted in presence of AgNPs. 20 µL of 2,4-dinitrophenol (0.01 M) solution were added to 1.7 mL of water in quartz cuvette, followed by 0.08 mL from AgNPs (1 mM) and 0.2 mL of $NaBH_4$ (0.1 M) into the mixture. The UV–Vis spectrum was recorded at room temperature (25 ℃). It was confirmed that there is no interference from other reagents at the selected λ_{max} for the investigated compounds. To be sure from the reducibility of our results in the catalytic experiments and calculating of rate constant for the catalytic reduction of 2,4-DNP to 2,4-DAP at room temperature and different temperatures, we repeat each experiment three times and standard deviation was calculated.

3 Results and discussion

3.1 Characterization of AgNPs

3.1.1 Spectral analysis

UV–Vis and surface plasmon resonance (S.P.R.) techniques were used to characterize AgNPs (Fig. 1). DRE extract contains a chemical component that acts as a reducing and capping agent, assists in the reduction of Ag^+ ions to form silver nanoparticles. The components of the extracts were indicated through the absorption bands recorded. The peak at 292 nm is attributed to the amino acid, while the peaks at 345 and 350 nm are characteristic for flavonoids and phenols. The amino acid that plays a role in the reduction and stability of nanoparticles has peaks at 459 and 442 nm in the spectra of DREAgNPs, MOEAg NPs, respectively [47–50]. The amino acid which plays a role in the reduction and stability of nanoparticles due to the chemical interaction between their groups (-COO-) and the metals. The types of interactions can be identified by measuring the difference in wavenumber (Δ) between the asymmetric and symmetrical stretching of the bands (-COO-). The chemical interaction is between lone pair of electrons on groups (-COO-) and the Ag. The broad bands centered on ≈ 450 nm are most probably due to aggregated AgNPs. The green rapid biogenic synthesis of AgNPs using Bauhinia variegata plant demonstrated. UV study reveals the final conformation for the formation of AgNPs by Intense Surface Plasmon Resonance (SPR) band at 452 nm. Also the reducing potential of Artemisia vulgaris leaves extract (AVLE) was investigated for synthesizing of AgNPs. The appearance of blackish brown color evidenced the complete synthesis of nanoparticles. The synthesized AgNPs were characterized by UV–Vis spectroscopy, UV–Vis absorption profile of the bio-reduced sample elucidated the main peak around 452 nm.

3.1.2 FT-IR analysis

Delonix regia extract (DRE), DREAgNPs, *Moringa oliefera* extract (MOE) and MOEAgNPs were analyzed (Fig. 2) and their spectra clarify the functional groups in the compounds. A peak indicative for cellulose was found in the 1000–1200 cm^{-1} region. A peaks appeared at 3298, 3307 cm^{-1} due to O–H and -NH groups, indicating the presence of flavanols in *Delonix regia* and *Moringa oliefera* extract, respectively. The shift in the position of the peak to 3264, 3200 cm^{-1} in the spectrum of the DREAgNPs and MOEAgNPs, respectively indicates the binding of Ag^+ ions with amino and hydroxyl groups. The band appeared

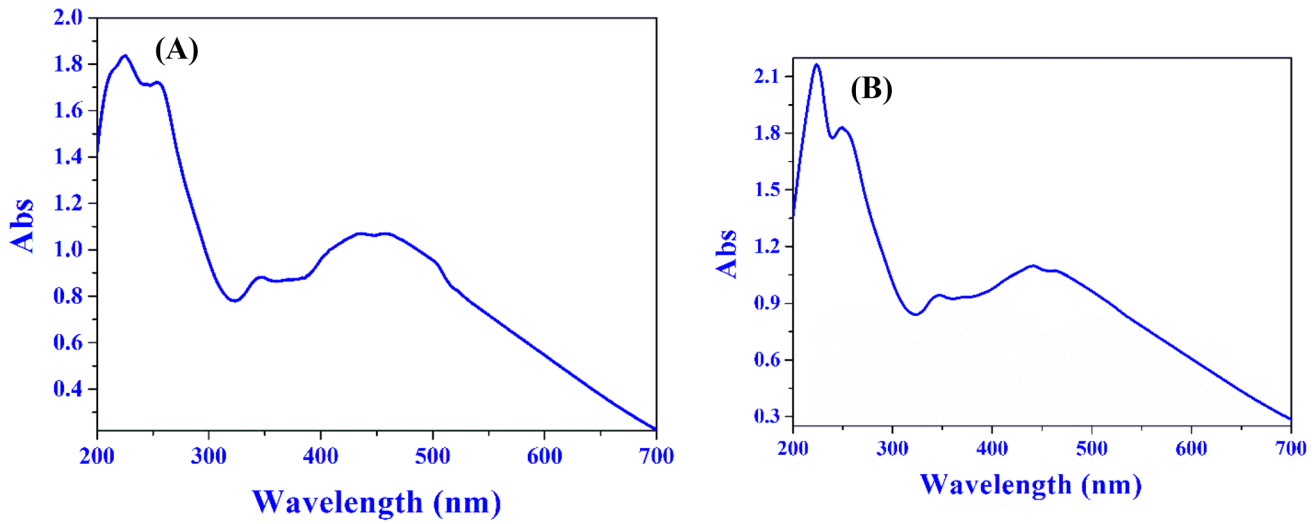

Fig. 1 UV–Vis spectra of **A** DREAgNPs and **B** MOEAgNPs

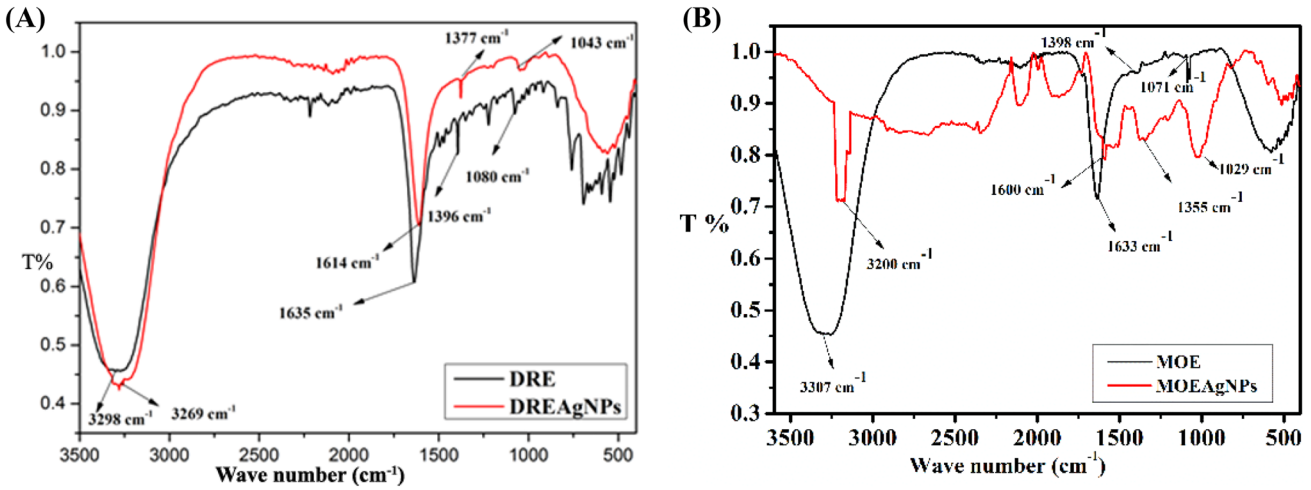

Fig. 2 FT-IR spectra of **A** DRE, DREAgNPs and **B** MOE, MOEAgNPs

at 1080, 1071 cm^{-1} is due to C-N stretch and the shift to 1043, 1029 cm^{-1} because of binding Ag^{+} ions with the C-N group in DREAgNPs and MOEAgNPs, respectively. Peaks were observed at 1635, 1633 cm^{-1} due to the amide bond of proteins arise from the carbonyl stretching, and is shifted to wavenumber at 1614, 1600 cm^{-1} indicates the binding of Ag^{+} ions with carbonyl groups in DREAgNPs and MOEAgNPs, respectively. The spectra displayed bands at 1396, 1398 cm^{-1} which attributed to the stretching of –C–O and –C–O–C that shifted to 1377, 1355 cm^{-1} after Ag^{+} ions binding. This confirms the bonding between Ag^{+} and –OH/COO– groups at protein in DREAgNPs and MOEAgNPs, respectively [5, 17, 31]. The synthesized DREAgNPs and MOEAgNPs show many peaks present in the DRE and MOE s due to the phytochemical compound in the *Delonix regia* and *Moringa oliefera* extracts as capping and reducing agent of Ag^{+} to Ag^{0} [5, 17, 31, 47–50].

3.1.3 XRD analysis of the silver nanoparticles

The crystal structure of AgNPs was determined using XRD. The peak values in Fig. 3 reveal that the XRD pattern of AgNPs has an FCC form and crystalline lattice at 2θ of 38°, 44°, 64° and 77° corresponding to (111), (200), (220), and (311) reflections of AgNPs, and these planes correspond to the standard JCPDS, file number 04-0783.

3.1.4 TEM analysis

This technique was used to examine the morphology and particle size of AgNPs. The majority of particles were spherical (Fig. 4a, c) and the size distribution may be seen in the photograph (Fig. 4b, d). The mean value of size in MOEAgNPs was 37 nm, while in DREAgNPs the size was

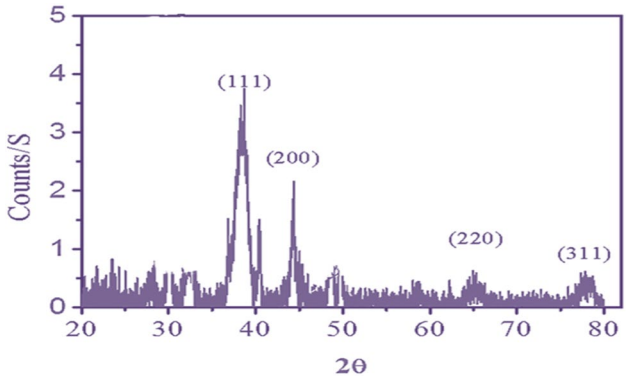

Fig. 3 XRD pattern of synthesized AgNPs

46 nm. Figure S1 shows high resolution TEM for the prepared MOEAgNPs confirms the purity and crystallinity of the prepared AgNPs. Moreover, d-spacing between crystallographic planes confirms nano size of the prepared Ag^{o}.

3.2 Adjusting the suitable conditions for green synthesis of AgNPs

According to operating parameters, the time needed for color change and the intensity of such color was varied from experiment to another. So, to establish the best conditions for AgNPs creation, the method variables must be adjusted. The concentration of either plant extract or silver ion, as well as the synthesis duration, was the parameters that need optimization. The particle size distributions in AgNPs generated were determined using dynamic light scattering (DLS) in each experiment. The impact of each variable on the particle size at any triple-level was computed. The figures show how the size of

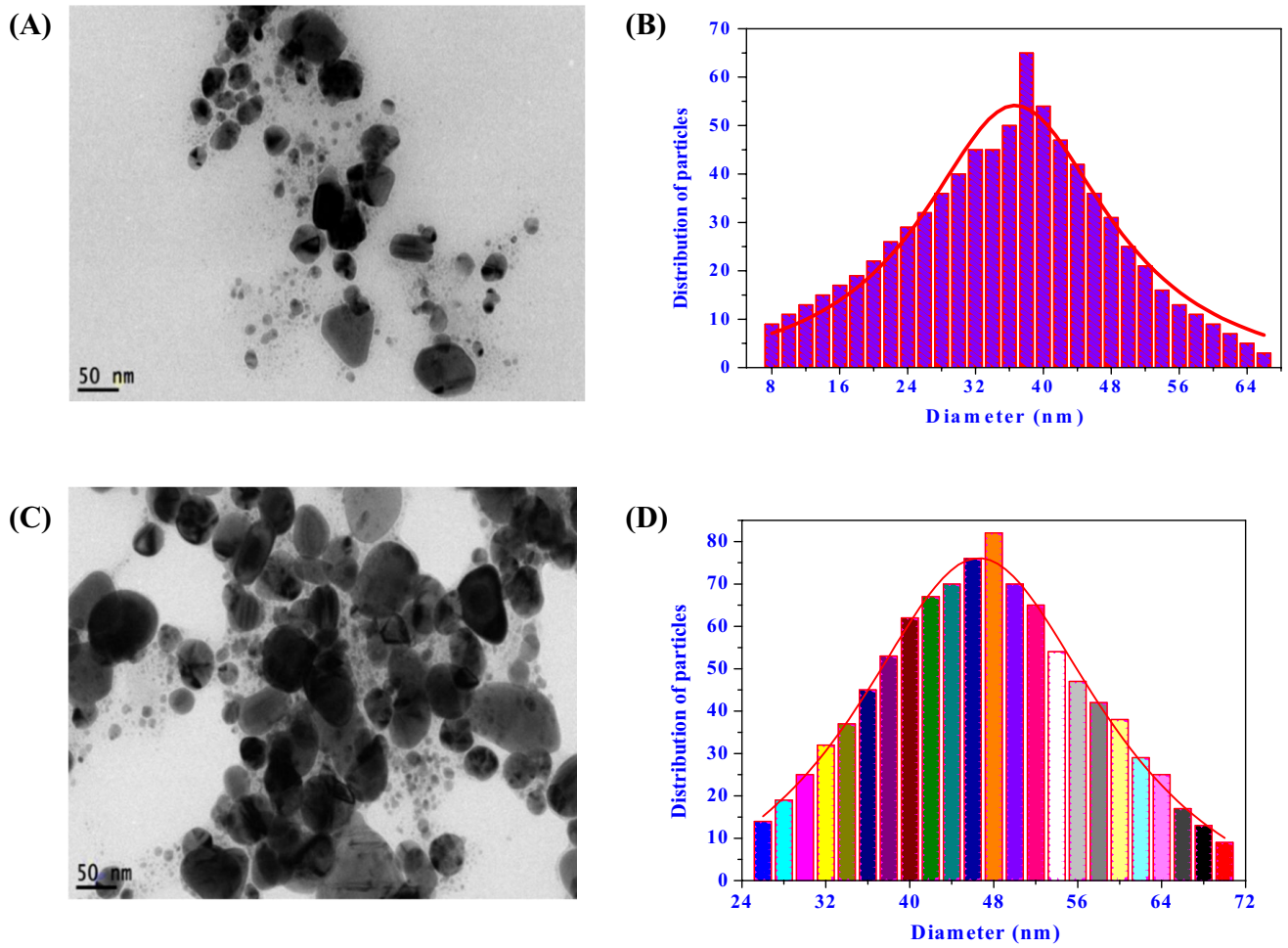

Fig. 4 TEM images and particle size distribution of **a**, **b** MOEAgNPs and **c**, **d** DREAgNPs

generated particles changes with the level rises or falls. The average effect of the variables exhibited the impact of plant quantity as changing the amount from 5 to 10 (w/v) reduces the size of silver particles, while increasing the amount to 15% increases the size of silver particles. Also, increasing the silver ion concentration from 1 to 2 mM leads to smaller silver particles, while increasing its concentration from 2 to 3 mM leads to the opposite trend. Furthermore, raising the synthesis time from 10 to 24 h causes a decrease in the particle size of silver. Whereas improving the temperature of plant extraction from 25 to 40 °C increases the size, but at 60 °C decreases the size of silver particles. Finally, except for the amount of plant used, the Ag^+ concentration, time and temperature inference the size of Ag^+ particles [51]. Consequently, the ideal conditions for such green synthesis are 2 mM Ag^+ concentration, 24 h time, and 60 °C temperature (Table 1, Fig S2).

3.3 Application of AgNPs in catalytic reduction of 2,4-dinitrophenol and kinetic study

Nanoscale materials offer a unique utility as catalysts for chemical transformations that are ordinarily hampered by the reaction's high kinetic barrier [52]. Unlike bulk silver, which is inert as a catalyst at the macroscale, AgNPs can be used as a catalyst for a variety of chemical transformations [53, 54]. Catalytic reduction of 2,4-dinitrophenol (2,4-DNP) was examined using $NaBH_4$ at room temperature in presence of MOEAgNPs and DREAgNPs [55, 56]. Although the reduction of 2,4-dinitrophenol to 2,4-diaminophenol using aqueous $NaBH_4$ is thermodynamically favorable, the reaction is difficult due to the activation barrier between the donor and acceptor molecules. To overcome the activation barrier, the AgNPs accelerate this reaction by promoting electron relay from the donor BH_4^- to the acceptor 2,4-DNP. In the absence of silver

Table 1 Catalytic reduction of 2,4-dinitrophenol (2,4-DNP) without catalyst and using catalyst MOEAgNPs and DREAgNPs in presence of $NaBH_4$ at different cycles

Entry (cycle no.)	Conc. of 2,4-DNP (mM)	Conc. of $NaBH_4$ (mM)
Without catalyst	0.01	0.1
With catalyst MOEAgNPs (0.001 mM) 1	0.01	0.1
With catalyst MOEAgNPs (0.001 mM) 2	0.01	0.1
With catalyst MOEAgNPs (0.001 mM) 3	0.01	0.1
With catalyst MOEAgNPs (0.001 mM) 4	0.01	0.1
With catalyst MOEAgNPs (0.001 mM) 5	0.01	0.1
With catalyst MOEAgNPs (0.001 mM) 6	0.01	0.1
With catalyst MOEAgNPs (0.001 mM) 7	0.01	0.1
With catalyst DREAgNPs (0.001 mM) 1	0.01	0.1
With catalyst DREAgNPs (0.001 mM) 2	0.01	0.1
With catalyst DREAgNPs (0.001 mM) 3	0.01	0.1
With catalyst DREAgNPs (0.001 mM) 4	0.01	0.1
With catalyst DREAgNPs (0.001 mM) 5	0.01	0.1
With catalyst DREAgNPs (0.001 mM) 6	0.01	0.1
With catalyst DREAgNPs (0.001 mM) 7	0.01	0.1

nanoparticles, the UV–Vis spectrophotometer was used to monitor the reaction and the spectra were obtained following the addition of $NaBH_4$ to 2,4-dinitrophenol and the highest absorption peak at 362 nm was shown (Fig. S3). This peak could be ascribed to the electronic transition n-π* due to non-boding electrons (oxygen and nitrogen atoms) in the 2,4-dinitrophenol structure. The catalysis mechanism of 2,4-dinitrophenolate ion reduction was shown in the following equations:

$$BH_4^- + 2H_2O \rightarrow BO_2^- + 4H_2$$

This peak stayed relatively stable for half an hour, indicating that the reaction is difficult without the presence of a catalyst. Moreover, the peak at 362 nm remained stable for several days in the absence of any catalyst, and no decrease of 2,4-DNP was observed.

The catalytic activity of MOEAgNPs and DREAgNPs was followed by the UV–Vis spectra of 2,4-dinitrophenol in the presence of $NaBH_4$ in the range of 200–700 nm (Figs. S4, 5). The yellow color of the 2,4-DNP solution increased deeper by adding $NaBH_4$, and a red shift from 362 to 450 or 422 nm occurred due to the synthesis of 2,4-dinitrophenolate ions, according to the preliminary experiment [55]. As the amount of 2,4-dinitrophenol in the sample decreased, the peak at 362 nm reduced and new peaks appeared at 294 or 288 and 450 or 422 nm. It indicated the formation of 2,4-dinitrophenolate ion and 2,4-diaminophenol in the reaction solution. As 2,4-dinitrophenolate intermediate transformed into 2,4-diaminophenol, the absorption bands of the 2,4-dinitrophenolate ion was decreased and a new small band around 316 nm was formed, the spectrum became stable indicating the formation of 2,4-diaminophenol (DAP) in the reaction. The yellow appearance of the 2,4-DNP solution slowly disappeared and became pale orange in the presence of MOEAgNPs as a catalyst [34, 57, 58].

The changes in the intensity of the peak at 362 nm with time can be used to track the kinetics of this process quantitatively. Because the reaction was carried out at a higher concentration of $NaBH_4$ than 2,4-dinitrophenol and AgNPs, the rate constant can be expected to be independent on the concentration of $NaBH_4$. As a result, the reaction is classified as a first-order with regard to the concentration of 2,4-dinitrophenol. The following equation concentration can be used to describe the reaction kinetics:

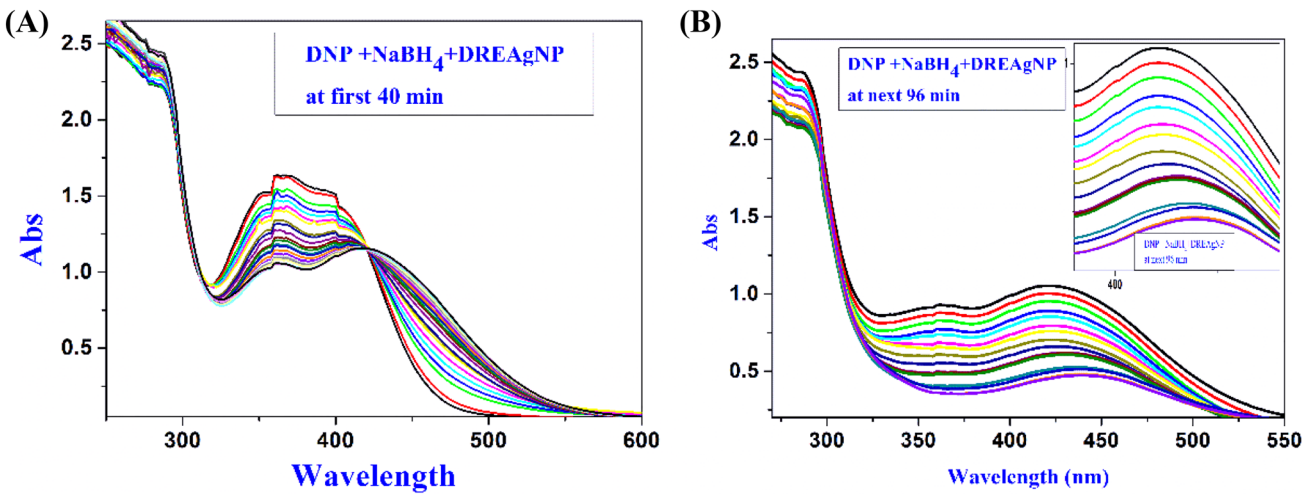

Fig. 5 UV–Vis spectra of the catalytic reduction of 2,4-dinitrophenol to the corresponding 2,4- diaminophenol by NaBH4 catalyzed by DRE AgNPs: **a** at first 40 min, **b** at next 96 min

$$\ln\frac{[A]}{[Ao]} = -kt$$

where k is the first-order rate constant, t is the reaction time, $[A_o]$ is the concentration of 2,4-dinitrophenols at time $t=0$ and $[A]$ is the concentration at time t. The value of $[A]$ can be obtained from the absorbance of the peak at 362 nm [59]. The decrease in intensity of the absorption peak at 362 nm overtime was used to compute the reaction rate constant. The change in the ratio ln A with time conforms the first-order kinetics equation, and the rate constant is determined from the linear relationship between ln A and time. From kinetic plots, the rate constants (k, min^{-1}) were found to be 1×10^{-3} min^{-1}, 42×10^{-3} min^{-1} and 26×10^{-3} min^{-1} for the reaction without any silver nanoparticles MOEAgNPs and with DREAgNPs respectively, Fig. S5. By comparing these rate constants values of 2,4-DNP reduction. AgNPs accelerated the reduction.

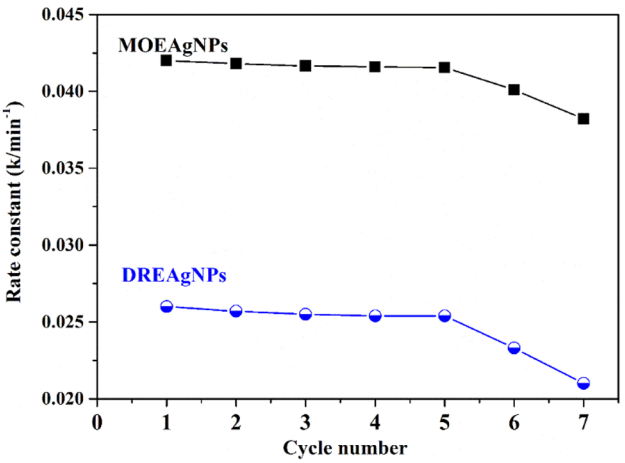

Fig. 6 Reaction rate constant for the reduction of 2,4-DNP catalyzed by the as-prepared MOEAgNPs and DREAgNPs catalyst for seven cycles

3.3.1 Recycling studies

The main advantage of heterogeneous catalysis system is the separation and possible reusability of the catalysts from the reaction system at the end of the reaction. Therefore, the reusability of the catalysts under study was further investigated. AgNPs were recovered from the reaction mixture by centrifugation and reused for catalytic reduction of 2,4-diaminophenol under comparable reaction conditions to assess the catalyst recycling capabilities. UV–Vis spectra were used to investigate the activity of MOEAgNPs and DREAgNPs in recycling capability within the catalytic reduction of 2,4-dinitrophenol to the corresponding 2,4-diaminophenol. Also, the rate constant of the reactions was calculated from the decrease in intensity of the absorption peak over time. The activity of the catalyst was expressed in terms of percentage activity by following the given relation.

$$\text{Percentage activity} = \frac{k\,(2\text{nd cycle})}{k\,(1\text{st cycle})} \times 100$$

where k(1 st cycle), the rate constants (k, min^{-1}) in the first cycle, k(2 nd cycle), the rate constants (k, min^{-1}) in successive cycles until cycle 7. (Fig. 6, Table 1).

The existence of an oxide layer over the surface of AgNPs on air exposure or small leaching of AgNPs during catalysis could explain the decrease in activity of nanocatalysts in the sixth cycle [60]. The slight decrease in sixth cycle (~4%) in the catalytic reuse of MOEAgNPs and (~9%) DREAgNPs catalyst, respectively, may be related to the clumping of surface supported Ag(0) nanoparticles, which reduces the number of active surface atoms. The 2,4-dinitrophenol solution has the greatest absorption bands at 362 nm, according to the previous results. Thus, in the absence of catalyst, the consumption rate of 2,4-dinitrophenols in presence of equivalent amounts of $NaBH_4$ was found to occur very slowly by the self-hydrolysis of sodium borohydride. However, in presence of a very low amount of AgNPs, the reduction of 2,4-dinitrophenols occur rapidly. The color of the reaction solutions changed from yellow to pale orange. The reduction of 2, 4-dinitrophenols in the presence of catalysts with excess $NaBH_4$ proceeds via the formation of diphenolate ions by the addition of $NaBH_4$ and the transformation of dinitrophenolate ions to diaminophenols [61–67]. The absorption bands of 2,4-dinitrophenol 362 nm shifted to 450 and 422 nm upon the addition of MOEAgNPs and DREAgNPs. This indicates the formation of 2,4-dinitrophenolate in the reaction solution and the intensities of their absorption bands gradually decreased as the reduction proceeds in the presence MOEAgNPs and DREAgNPs. The complete consumption of 2,4-dinitrophenols occurred within 36, 40 min using MOEAgNPs and DREAgNPs catalyst, respectively. Comparing of our results for the catalytic activity of AgNPs toward the reduction of 2,4-dinitrophenol, we found enhancing in the rate constant of the current study (Table 2), while the literature reported 8×10^{-3} min^{-1} [34] 13.5×10^{-3} min^{-1} [68] and 6.5×10^{-3} min^{-1} rates[58]

3.3.2 Thermodynamics of the reduction of 2, 4-dinitrophenol

We investigated the temperature-dependent reduction reaction of 2,4-dinitrophenol catalyzed by MOEAgNPs and DREAgNPs at different temperatures. The influence of temperature on the k values was investigated by altering the temperature from 293 to 313 K. The k values for the reduction of 2,4-dinitrophenol increase with the increase in temperature, as shown in Table 2 and Figures S6, S7. This

Table 2 Temperature dependent k values for the reduction of 2,4-dinitrophenol catalyzed by MOEAgNPs and DREAgNPs

Temperature (K)	k (min^{-1}) of 2,4-dinitrophenol reduction by MOEAgNPs $\times 10^{-3}$	k (min^{-1}) of 2,4-dinitrophenol reduction by DREAgNPs $\times 10^{-3}$
293	37 ± 0.17	24 ± 0.10
298	42 ± 0.21	26 ± 0.09
303	50 ± 0.24	28 ± 0.18
308	62 ± 0.19	40 ± 0.12
313	101 ± 0.20	55 ± 0.19

could be attributed to the increase in the diffusion of reactant molecules.

The activation energies (Ea) for the 2,4-dinitrophenol reduction process were calculated using the Arrhenius equation [69–72]:

$$\ln k = \ln A - E_a/RT$$

where E_a is the activation energy, A is the Arrhenius factor, T is absolute temperature and R is the ideal gas constant. The slope of the plot of ln k vs. $1/T$ was used to calculate Ea values, as shown in Figures S8, S9 (a, b) and Table S2. The activation parameters for the catalytic reduction of 2,4-dinitrophenol using AgNPs are summarized in Table S2.

The activation energies E_a for 2,4-dinitrophenol catalyzed by MOEAgNPs and DREAgNPs, are 36.4 and 31.7 kJ mol^{-1}, respectively, confirming that the reaction follows the L–H mechanism [73]. Activation enthalpy (ΔH^*) and activation entropy (ΔS^*) for the reduction of 2,4-dinitrophenol were determined using the Eyring equation.

$$\ln\left(\frac{k}{T}\right) = \ln\left(\frac{KB}{h}\right) + \frac{\Delta S*}{R} - \frac{\Delta H*}{RT}$$

$$\Delta G^* = \Delta H^* - T\Delta S^*$$

where k is the rate constant (min^{-1}), R is the universal gas constant, T is the temperature (K), h is the Plank constant, K_B is the Boltzmann constant and ΔG is the Gibbs free energy. The thermodynamic parameters ΔH^* and ΔS^* were obtained from Fig. S8 a, b and represented in Table S2. The values k constant for reduction of 2,4-dinitrophenol catalyzed by MOEAgNPs and DREAgNPs were 0.042 and 0.026 min^{-1}, respectively. Thermodynamic parameters in presence of MOEAgNPs catalyst such as activation enthalpy (ΔH^*) and activation entropy (ΔS^*) and Gibbs free energy (ΔG^*) for the reduction of 2,4-dinitrophenol were 34.1 kJ mol^{-1}, − 157.5 J mol^{-1} K^{-1}, 81.02 kJ mol^{-1}, respectively. On the other hand, thermodynamic parameters for the reaction in presence of DREAgNPs catalyst such as activation enthalpy (ΔH^*) and activation entropy (ΔS^*) and Gibb's free energy (ΔG^*) were 29.2 kJ mol^{-1}, − 177.02 J mol^{-1} K^{-1} and 82.01 kJ mol^{-1}, respectively. Combining entropy, enthalpy and Gibbs free energy, we can estimate whether a reaction will occur spontaneously. If the $G = 0$ indicates that the system is in equilibrium, $G < 0$ the process is spontaneous and the $G > 0$ for nonspontaneous process. This reaction will not proceed spontaneously at any temperature since $(\Delta H^*) > 0$ and $(\Delta S^*) < 0$. The opposite reaction, however, is kinetically inhibited. The negative value of (ΔS^*) indicates the decrease in randomness. The reduction of 2,4-DNP is a clearly an endothermic reaction, as shown in Table S2 [74]. To proceed with the reduction reaction, 2,4-dinitrophenol must first overcome the energy barrier by adsorbing on the catalyst surface. Hence, the MOEAgNPs and DREAgNPs show excellent catalytic activity toward the reduction of 2,4-dinitrophenol to 2,4-diaminphenol.

3.3.3 The mechanism of catalytic process

The acceptable mechanism for the reduction of 2,4-dinitrophenol in presence of Ag nanostructures was Langmuir–Hinshelwood (L–H) based, which is kinetically controlled [75]. This metallic nanostructure offers a broad surface accessible for the catalytic process to happen according to known mechanism [76, 77]. Accordingly, our catalytic reaction may behave the same path of reaction that proposed previously [75–77], in which, the reactants of 2,4-dinitrophenol and BH_4^- ions adsorbed on AgNPs surface and immediately the hydrogen species transferred to AgNPs then to the targeted compound (2,4-dinitrophenol). So, 2,4-aminophenol was formed through a stepwise reduction reaction which was completed in six steps (Schemes 1, 2). This heterogeneous catalytic reaction was facilitated via AgNPs, which help in H_2 atomization after adsorption that transferred to reduce the target. The catalytic reduction reaction k values are proportional to the materials surface area. With a rise in the concentration of 2,4-dinitrophenol, the number of molecules adsorbed at the surface of the AgNPs increases and the surface becomes saturated with 2,4-dinitrophenol molecules. This lowers the rate of hydrogen transfer from the BH_4^- ions to the targeted molecule. This confirms the catalytic role of AgNPs in the reduction reaction, which occurs according to L–H mechanism [75].

3.3.3.1 Computational confirmation The reactant (2,4-dinitrophenol) and the product (2,4-diaminophenol)

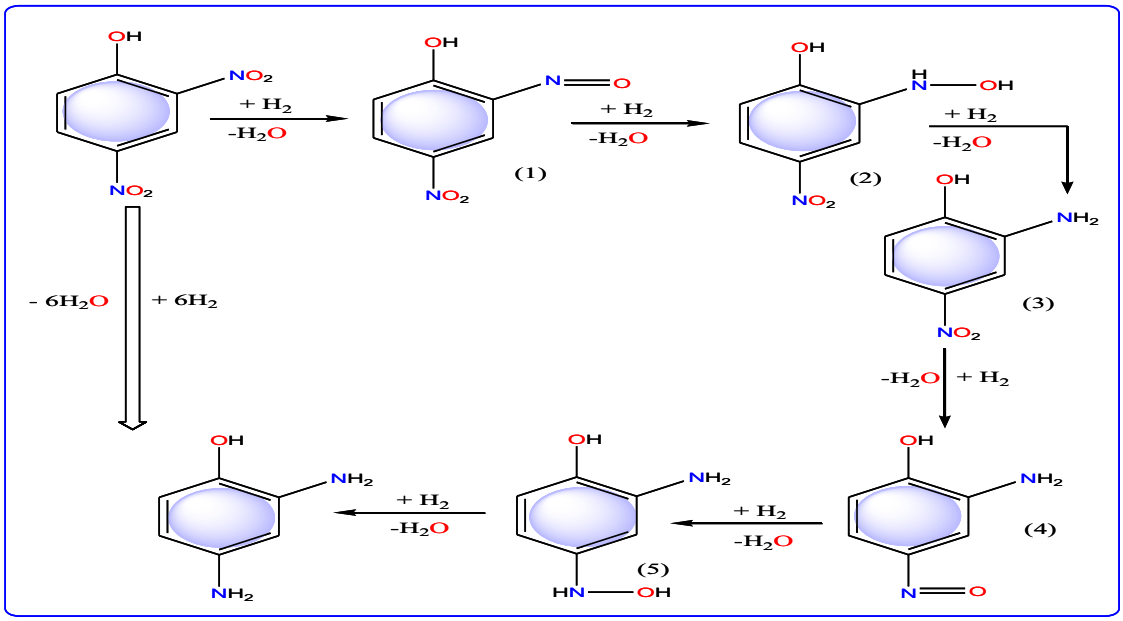

Scheme 1 The suggested catalytic protocol of AgNPs toward the reduction of 2,4-dinitrophenol by BH_4^-

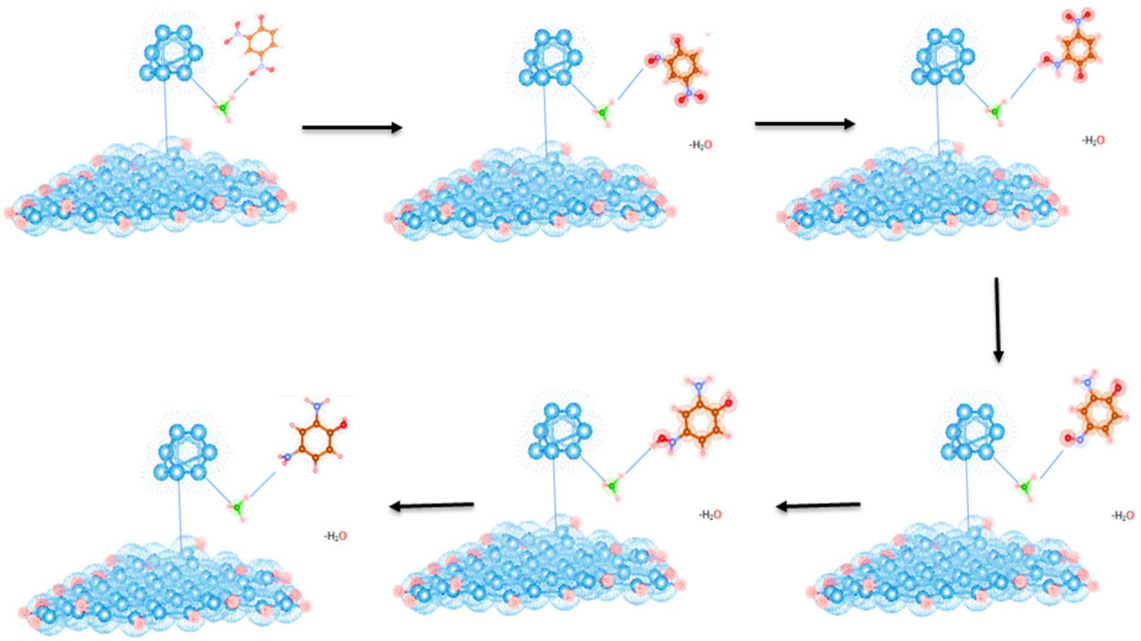

Scheme 2 A simulation for AgNPs surface interaction during the stepwise reduction process

as well as the suggested intermediates formed in this catalyzed reaction were optimized to estimate essential physical parameters. This was performed via Gaussian 09 software [78] using DFT/B3LYP and under valence double-zeta, which includes polarizing function (6-31G*) [79]. This basis set utilized polarization function over valence double-zeta (6-31G*) via DFT method and using Becke3–Lee–Yang–Parr (B3LYP) correlation exchange [80]. The double-zeta functions is essential for the equivalent orbitals, even though they are completely different in the molecule.

The compounds in different views as well as their HOMO and LUMO levels were obtained and displayed (Table S3). In addition, the energy values for the frontier orbitals as well as the energy gap in between (ΔE (ev) = $E_{LUMO} - E_{HOMO}$)

Table 3 Computational outputs from optimization process using DFT method

Compound, energy (eV)	HOMO	LUMO	Vertical view	Horizontal view
2,4-dinitrophenol HOMO = -0.22979 LUMO = -0.18209 ΔE = -0.0477 E = -712.02 a. u.	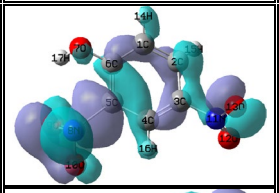	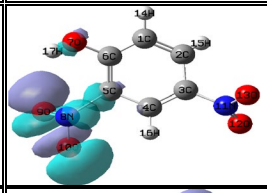	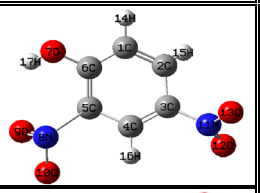	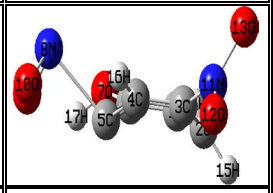
Intermediate (1) HOMO = -0.21448 LUMO = -0.1039 ΔE = -0.1106 E = -637.59 a. u.	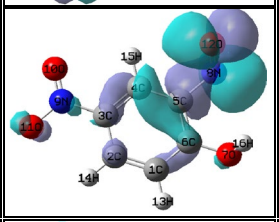	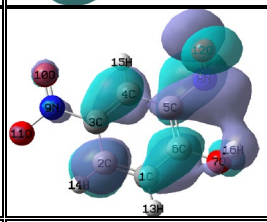	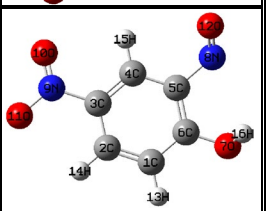	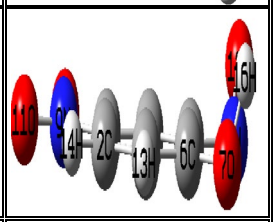
Intermediate (2) HOMO = -0.1863 LUMO = -0.06351 ΔE = -0.1228 E = -638.81 a. u.	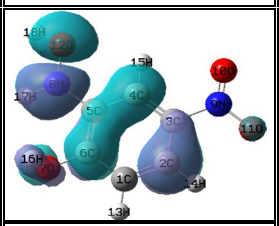	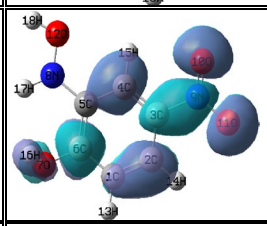	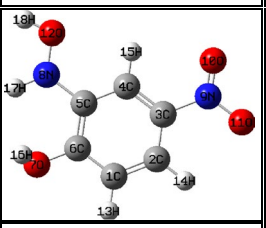	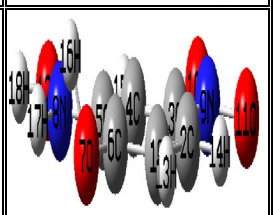
Intermediate (3) HOMO = -0.21505 LUMO = -0.06797 ΔE = -0.1471 E = -564.11 a. u.	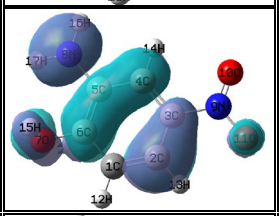	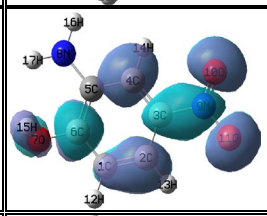	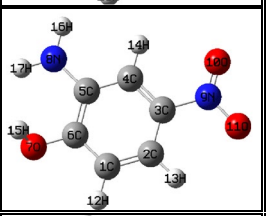	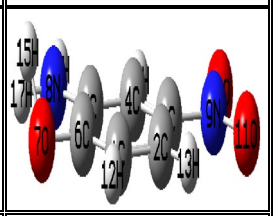
Intermediate (4) HOMO = -0.17642 LUMO = -0.06708 ΔE = -0.1093 E = -489.33 a. u.	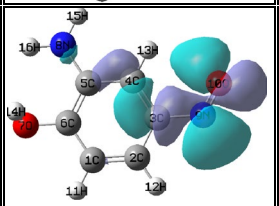	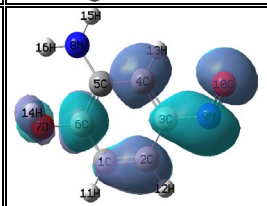	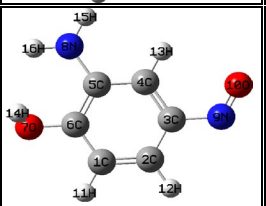	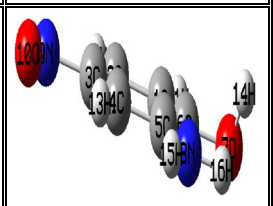
Intermediate (5) HOMO = -0.13913 LUMO = -0.01602 ΔE = -0.1231 E = -490.53 a. u.	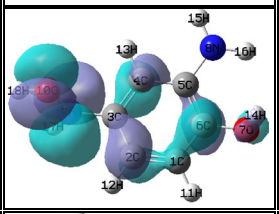	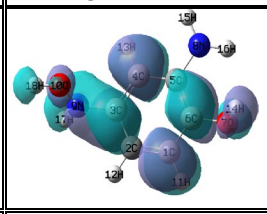	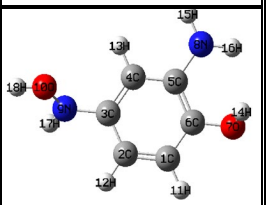	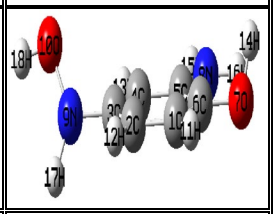
2,4-diaminophenol HOMO = -0.17597 LUMO = -0.01882 ΔE = -0.15715 E = -415.83 a.u.	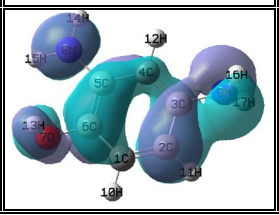	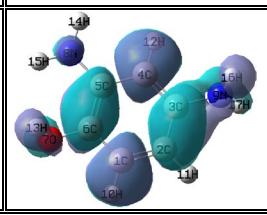	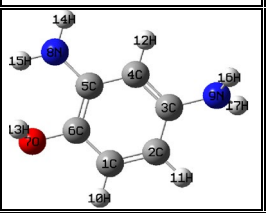	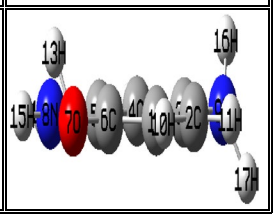

were also displayed (Table 1) [81–84]. The ΔE appeared lower in 2,4 dinitrophenol, which indicates the liability of outer orbital electrons, also facilitated electronic transitions. This feature is preferable for reduction process of such compound. Also, all intermediates exhibited reduced energy gap values, which reflect the same indication and the reduction process is easy from step to another till consuming 6 H_2 molecules. On the other hand, the energy gap value is high in 2,4-diaminophenol, which indicates the high stability of its electronic configuration as well as its inability

for extra- reduction. Furthermore, the energy contents of the reactant or intermediates are high than the energy level of the product (see Table 3). This indicates this reduction reaction is thermodynamically fevered through exothermic process. Also, the activation energy barriers are not high and the transformation reaction is fast and the reactant (2,4-diaminophenol) is kinetically labile. This indicates the influence of AgNPs on facilitating the reaction under mild condition of activation. This is easily noticed from the optimum temperature used (60 ℃) [85]. Moreover, the estimated bond lengths, bond angles and charges (Table S3) agree with the characteristics of bonds and the hybridization of central atoms inside all the structures. Also, the intermediate compounds from 1 to 5 are highly closer in their bond lengths and angles which reflects their similarity in energy content and the ease of their transformations. The nucleophilic or electrophilic characteristics of the substituted groups was clearly discriminated based on their charges recorded.

4 Conclusion

The biosynthesis of MOEAgNPs and DREAgNPs utilizing *M. oleifera* and *Delonix regia* extracts was demonstrated in this study. According to FT-IR and UV–Vis spectra, phytochemical compounds in the plant extract, such as amino acids and flavanols, were responsible for the bio reduction of Ag^+ ions to Ag^0. The size and morphology of AgNPs were indicated using TEM image. At low temperatures, the produced MOEAgNPs and DREAgNPs were used to reduce 2,4- dinitrophenol to 2,4-diaminophenol using $NaBH_4$. In terms of catalytic reduction of 2,4-dinitrophenol, the performance of AgNPs was evaluated based on spectral studies. All the results demonstrated the AgNPs that under mild conditions have high catalytic efficiency toward the reduction of 2,4-dinitrophenol by $NaBH_4$. By centrifugation, MOEAgNPs and DREAgNPs were isolated from the reaction mixture and reused for another process. The activation energies for 2,4-dinitrophenol catalyzed by MOEAgNPs and DREAgNPs, respectively, are 36.4 and 31.7 kJ mol^{-1} which confirms L–H reaction mechanism. Thermodynamic parameters such as activation enthalpy (ΔH^*) and activation entropy (ΔS^*) and the Gibb's free energy (ΔG^*) for the reduction of 2,4-dinitrophenol were 34.1, − 157.5, 81.02 kJ mol^{-1}, respectively, for MOEAgNPs catalyst. While, for DREAgNPs catalyst were 29.2, − 177.02 and 82.01 kJ mol^{-1}, respectively. The catalysis mechanism was suggested based on stepwise reaction. This mechanism was supported through DFT studies for the reactant and product as well as the suggested intermediates.

Supplementary Information The online version contains supplementary material available at https://doi.org/10.1007/s00339-022-05704-9.

Acknowledgements Dr. Mohamed acknowledge Taif University Researchers Supporting Project number (TURSP-2020/43). Taif University, Taif, Saudi Arabia.

Data availability All relevant data are within the manuscript and available from the corresponding author upon request.

Declarations

Conflict of interest The authors declare no conflict of interest.

References

1. Z.M. Qi, H.S. Zhou, N. Matsuda, J. Phys. Chem. B **108**, 7006 (2004)
2. J. Amici, C. Torchio, D. Versaci, D. Dessantis, A. Marchisio, F. Caldera, F. Bella, C. Francia, S. Bodoardo, Polymers **13**, 1625 (2021)
3. S. Horta-Piñeres, R. Britto Hurtado, D. Avila-Padilla, Appl. Phys. A **126**, 15 (2020)
4. M.A.A.M. Abdah, M. Mokhtar, L.T. Khoon, K. Sopian, N.A. Dzulkurnain, A. Ahmad, Y. Sulaiman, F. Bella, M. SukorSuait, Energy Rep. **7**, 8677 (2021)
5. P. Mohanpuria, N.K. Rana, S.K. Yadav, J. Nanoparticle Res. **103**, 507 (2008)
6. K.-H. Cho, J.-E. Park, T. Osaka, S.-G. Park, Electrochim. Acta **51**, 956 (2005)
7. R.O. Becker, Met.-Based Drugs **6**, 311 (1999)
8. A.M. Abu-Dief, L.H. Abdel-Rahma, M.A. Abd-El Sayed, M.M. Zikry, A. Nafady, ChemistrySelect **5**, 13263 (2020)
9. G. Borkowand, J. Gabbay, Curr. Chem. Biol. **3**, 272 (2009)
10. G. Borkow, J. Gabbay, FASEB J. **18**, 1728 (2004)
11. J. Ma, H. Wong, L.B. Kong, K.W. Peng, Nanotechnology **14**, 619 (2003)
12. K. Chaloupka, Y. Malam, A.M. Seifalian, Trends Biotechnol. **28**, 580 (2010)
13. O.V. Salata, J. Nanobiotechnol. **2**, 1 (2004)
14. R. Tankhiwale, S. Bajpai, Colloids Surf. B. **9**, 164 (2009)
15. T.V. Duncan, J. Colloid Interface Sci. **363**, 1 (2011)
16. D.T. Dubas, P. Kumlangdudsana, P. Potiyaraj, Colloids Surf. A **289**, 105 (2006)
17. B. Ajitha, Y.A.K. Reddy, S. Shameer, K.M. Rajesh, Y. Suneetha, P.S. Reddy, J. Photochem. Photobiol. B **149**, 84 (2015)
18. K. Mallick, M. Witcomb, M. Scurrell, Mater. Chem. Phys. **97**, 283 (2006)
19. S. Ahmed, M. Ahmad, B.L. Swami, S. Ikram, J. Adv. Res. **7**, 17 (2016)
20. G. Zhang, F. Zhang, H. Morikawa et al., Appl. Phys. A **114**, 127 (2014)
21. T. Ranjeth Kumar Reddy, H.J. Kim, Appl. Phys. A **122**, 652 (2016)
22. L.S.B. Upadhyay, N. Verma, Anal. Lett. **48**, 2676 (2015)
23. S.K. Kanawaria, A. Sankhla, P.K. Jatav, Appl. Phys. A **124**, 320 (2018)
24. A. Neog, P. Das, R. Biswas, Appl. Phys. A **127**, 913 (2021)
25. C.R.B. Lopes, D.S. Junior, F.R.D. Silva, Appl. Phys. A **127**, 244 (2021)
26. H. Bar, D.K. Bhui, G.P. Sahoo, P. Sarkar, S.P. De, A. Misra, Colloids Surf. A **339**, 134 (2009)
27. S. Li, Y. Shen, A. Xie, X. Yu, L. Qiu, L. Zhang, Q. Zhang, Green Chem. **9**, 852 (2007)
28. A. Singh, D. Jain, M. Upadhyay, N. Khandelwal, H. Verma, Dig. J. Nanomater. Biostructures **5**, 483 (2010)

29. G. Singhal, R. Bhavesh, K. Kasariya, A.R. Sharma, R.P. Singh, J. Nanopart. Res. **13**, 2981 (2011)
30. A. Saxena, R.M. Tripathi, F. Zafar, P. Singh, Mater. Lett. **67**, 91 (2012)
31. D. Philip, Physica E **42**, 1417 (2010)
32. R. Zhou, M.P. Srinivasan, J. Environ. Chem. Eng. **3**, 609 (2015)
33. C.M. Park, J. Heo, Y. Yoon, Chemosphere **168**, 617 (2016)
34. K. Gerelbaatar, A. Tsogoo, R. Dashzeveg, N. Tsedev, E.O. Ganbold, Solid State Phenom. **271**, 76 (2017)
35. F.A. Al-Marhaby, R. Seoudi, World J. Nano Sci. Eng. **6**, 29 (2016)
36. U. Kurtan, A. Baykal, Mater. Res. Bull. **60**, 79 (2014)
37. E. Karaoglu, M.M. Summak, A. Baykal, H. Sözeri, M.S. Toprak, J Inorg Organomet Polym **23**, 409 (2013)
38. E. Karaoglu, U. Özel, C. Caner, A. Baykal, M.M. Summak, H. Sözeri, Mater. Res. Bull. **47**, 4316 (2012)
39. M. Demirelli, E. Karaoglu, A. Baykal, H. Sozeri, J Inorg Organomet Polym **23**, 1274 (2013)
40. Y. Lu, X. Wan, L. Li, P. Sun, G. Liu, J. Mater. Res. Technol. **12**, 1832 (2021)
41. C. Baiano, E. Schiavo, C. Gerbaldi, F. Bella, G. Meligrana, G. Talarico, P. Maddalena, M. Pavone, A.B. Muñoz-García, Molecular Catalysis **496**, 111181 (2020)
42. F. Bella, S. De Luca, L. Fagiolari, D. Versaci, J. Amici, C. Francia, S. Bodoardo, Nanomaterials **11**, 810 (2021)
43. O.M. Bankole, T.D. Olorunsola, A.S. Ogunlaja, J. Photochem. Photobiol. **15**, 112934 (2021)
44. Y. Slimani, M.A. Almessiere, I.A. Auwal, S.E. Shirsath, M.A. Gondal, M. Sertkol, A. Baykal, Arab. J. Chem. **14**, 103261 (2021)
45. R.A. Dakheel, S. Rehman, M.A. Almessiere, F.A. Khan, M.A. Gondal, A. Mostafa, A. Baykal, Pharmaceuticals **13**(8), 193 (2020)
46. J.Y. Song, B.S. Kim, Bioprocess and Biosystems. Engineering **32**, 79–84 (2009)
47. A.M. Abu-Dief, L.H. Abdel-Rahma, M.A. Abd-El Sayed, M.M. Zikry, AJACR **9**, 1 (2021)
48. L.H. Abdel-Rahma, A.M. Abu-Dief, M.A. Abd-El Sayed, M.M. Zikry, J. Chem. Mater. Res. **8**(4), 8 (2016)
49. L.H. AbdelRahma, A.M. AbuDief, M.A. Abd-ElSayed, M.M. Zikry, J. Trans. Met. Complex. **1**, 10 (2018)
50. L.H. Abdel-Rahma, A.M. Abu-Dief, M.A. Abd-El Sayed, M.M. Zikry, Arch Chem Res. **1**, 1 (2016)
51. S.M. Pourmortazavi, M. Taghdiri, V. Makari, M. Rahimi-Nasrabadi, Spectrochim. Acta Part A Mol. Biomol. Spectrosc. **136**, 1249 (2015)
52. S. Kim, W.B. Sang, J.S. Lee, J. Park, Tetrahedron **65**, 1461 (2009)
53. M. Pan, J. Gong, G. Dong, C.B. Mullins, Acc Chem Res **46**, 650 (2013)
54. J. Gong, C.B. Mullins, Acc Chem Res **42**, 1063 (2009)
55. N. Pradhan, A. Pal, T. Pal, Colloids Surf. A **196**, 247 (2002)
56. K. Kuroda, T. Ishida, M. Haruta, J. Mol. Catal. A Chem. **298**, 7 (2009)
57. X.-Q. Wu, X.-W. Wu, Q. Huang, J.-S. Shen, H.-W. Zhang, Appl. Surf. Sci. **331**, 210 (2015)
58. K. Karakas, A. Celebioglu, M. Celebi, T. Uyar, M. Zahmakiran, Appl. Catal. B **203**, 549 (2017)
59. M. Gondwal, G.J. Pant, Int. J. Biomater. **2018**, 6735426 (2018)
60. K. Naseem, R. Begum, W. Wu, A. Irfan, A.G. Al-Sehemi, Z.H. Farooqi, J. Clean. Prod. **211**, 855 (2019)
61. S. Xiao, M. Shen, R. Guo, S. Wang, X. Shi, J. Phys. Chem. C **113**, 18062 (2009)
62. X. Fang, H. Ma, S. Xiao, M. Shen, R. Guo, X. Cao, X. Shi, J. Mater. Chem. **21**, 4493 (2011)
63. Y. Huang, H. Ma, S. Wang, M. Shen, R. Guo, X. Cao, M. Zhu, X. Shi, A.C.S. Appl, Mater. Interfac. **4**, 3054 (2012)
64. E. Formo, E. Lee, D. Campbell, Y. Xia, Nano Lett. **8**, 668 (2008)
65. P. Zhang, C. Shao, Z. Zhang, M. Zhang, J. Mu, Z. Guo, Y. Liu, Nanoscale **3**, 3357 (2011)
66. V. Thavasi, G. Singh, S. Ramakrishna, Energy Environ. Sci. **1**, 205 (2008)
67. Y. Lu, X. Wan, L. Li, P. Sun, G. Liu, J. Market. Res. **12**, 1832 (2021)
68. R. Makaudi, H.K. Paumo, B.K. Pone, L. Katata-Seru, Polymers **13**(21), 3800 (2021)
69. A.D.M. Mohamad, M.J.A. Abualreish, A.M. Abu-Dief, Can. J. Chem. **99**, 763–772 (2021)
70. S. Saha, A. Pal, S. Kundu, S. Basu, T. Pal, Langmuir **26**, 2885 (2010)
71. E.A. Abu-Gharib, R. El-Khatib, L.A.E. Nassr, A.M. Abu-Dief, Arab J. Chem. **10**, S988–S995 (2017)
72. E.A. Abu-Gharib, R.M. El-Khatib, L.A.E. Nassr, A.M. Abu-Dief, J. Korean Chem. Soc. **55**(3), 346–353 (2011)
73. M.A. Mahmoud, F. Saira, M.A. El-Sayed, Nano Lett. **10**, 3764 (2010)
74. H. Zendah, I. Khattech, J. Chem. Thermodyn. **87**, 29 (2015)
75. S. Wunder, F. Polzer, Y. Lu, Y. Mei, M.J. Ballauff, J. Phys. Chem. C **114**, 8814 (2010)
76. Y. Zhang, Z. Cui, L. Li, L. Guo, S. Yang, Phys. Chem. Chem. Phys. **17**, 14656 (2015)
77. S.R. Thawarkar, N.D. Khupse, A. Kumar, ChemistrySelect **2**, 6833 (2017)
78. M. Frisch, G. Trucks, H. Schlegel, G.S. Znseria, M. Robb, J. Cheeseman, G. Scalmani, V. Barone, B. Mennucci, G. Petersson (eds.), *Gaussian 09 Revision A. 1* (Gaussian Inc, Wallingford, 2009)
79. M.A.E.A.A. El-Remaily, T. El-Dabea, M. Alsawat, M.H.H. Mahmoud, A.A. Alfi, N. El-Metwaly, A.M. Abu-Dief, ACS Omega **32**, 21071 (2021)
80. C. Lee, W. Yang, R.G. Parr, Development of the Colle-Salvetti correlation-energy formula into a functional of the electron density. Phys. Rev. B **37**(2), 785–789 (1988)
81. S.J. Almehmadi, A. Alharbi, M.M. Abualnaja, K. Alkhamis, M. Alhasani, S.H. Abdel-Hafez, R. Zaky, N.M. El-Metwaly, Arb. J. Chem. **15**(1), 103586 (2022)
82. A.M. Abu-Dief, R.M. El-khatib, F.S. Aljohani, S.O. Alzahrani, A. Mahran, M.E. Khalifa, N.M. El-Metwaly, J. Mol. Struct. **1242**, 130693 (2021)
83. S.D. Al-Qahtani, A. Alharbi, M.M. Abualnaja, A. Hossan, M. Alhasani, A.M. Abu-Dief, M. Khalifa, N. El-Metwaly, J. Mol. Liq. **349**, 118100 (2022)
84. E.T. Aljohani, M.R. Shehata, F. Alkhatib, S.O. Alzahrani, A.M. Abu-Dief, Appl. Organom. Chem. **35**(5), e6154 (2021)
85. F.S. Aljohani, A.M. Abu-Dief, R.M. El-Khatib, H.A. Al-Abdulkarim, A. Alharbi, A. Mahran, M.E. Khalifa, N.M. El-Metwaly, J. Mol. Struct. **1246**, 131139 (2021)